Materials & Design 215 (2022) 110473

Contents lists available at ScienceDirect

Materials & Design

journal homepage: www.elsevier.com/locate/matdes

Derivation of material properties using small punch and shear punch test methods

R.J. Lancaster *, S.P. Jeffs, B.J. Haigh, N.C. Barnard

Institute of Structural Materials, College of Engineering, Bay Campus, Swansea University, Swansea SA1 8EN, United Kingdom

HIGHLIGHTS

- Empirical expressions to predict tensile and yield strength by means of small punch and shear punch testing have been validated.
- Data generated through shear punch testing found to more accurately correlate with uniaxial tensile properties.
- Finite element modelling accurately captured the deformation behaviour in both test types.
- Ti-6Al-4V found to be unsuitable for SP testing due to HCP crystal structure, less available slip systems and reduced ductility.

GRAPHICAL ABSTRACT

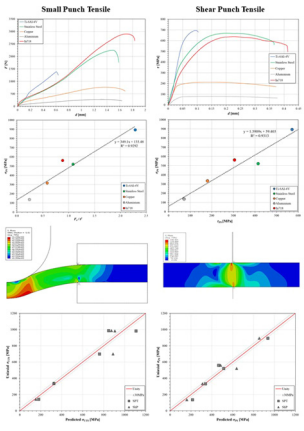

ARTICLE INFO

Article history:
Received 8 December 2021
Revised 9 February 2022
Accepted 14 February 2022
Available online 24 February 2022

ABSTRACT

The Small Punch (SP) and Shear Punch (ShP) tests are well established mechanical test approaches that have found application in several industrial sectors for material ranking and mechanical property estimation, particularly where more conventional approaches are inhibited. Despite the advantages that the two test methodologies have to offer, the main drawback is the complex understanding of the mechanical data generated from the experiments and how it can be correlated to more recognised properties. Typically, the most desired properties relate to the uniaxial properties of yield stress, ultimate tensile strength and ductility, but to date, there is no single robust and overarching approach for correlating such properties for a wide array of metallic materials that exhibit varying levels of ductility. This paper will for the first time directly compare properties obtained from a series of uniaxial tensile, SP and ShP tests across several metallic materials, and look to establish and correlate equivalent properties across the different test types. The materials investigated range from commercially pure entities to more advanced alloy systems. The generated results, empirical relationships and numerical simulations will inform which materials can be correlated across the different test regimes, and identify why the relationship in certain materials breaks down.
© 2022 The Authors. Published by Elsevier Ltd. This is an open access article under the CC BY license (http://creativecommons.org/licenses/by/4.0/).

1. Introduction

Mechanical property assessment is a fundamental stage in the materials selection process when considering new alloys for any structural component. However, to perform an extensive mechan-

* Corresponding author.
E-mail addresses: r.j.lancaster@swansea.ac.uk (R.J. Lancaster), s.p.jeffs@swansea.ac.uk (S.P. Jeffs), 823458@swansea.ac.uk (B.J. Haigh), n.c.barnard@swansea.ac.uk (N.C. Barnard).

https://doi.org/10.1016/j.matdes.2022.110473
0264-1275/© 2022 The Authors. Published by Elsevier Ltd.
This is an open access article under the CC BY license (http://creativecommons.org/licenses/by/4.0/).

ical characterisation of any novel material at the development stage can be an expensive activity when accounting for the relatively large volume of material required and likely restricted material availability. Such scenarios have led to the development of smaller scale test procedures. One particular test methodology is the small punch (SP) test, an experimental approach derived in the 1980s to assess in-service degradation of nuclear reactor components exposed to irradiation damage [1] and to provide an indication of the residual lifetime of the material for further safe operation. With time, the SP test technique has seen increased adoption, with research now available for the application of the test approach in alternative industrial sectors such as aerospace [2] and automotive [3] and to assess the properties of more advanced novel materials such as single crystal superalloys [4] and those fabricated by additive manufacturing (AM) [5,6].

In response to the increased use of SP testing in worldwide laboratories, a European Code of Practice (EUCoP) for SP tensile, fracture and creep testing was developed early in the 21st century and launched by CEN in 2006 [7]. This has since been formulated into both a European Norm (EN) and an ASTM equivalent standard, following an increased uptake in the use of the test methodologies and extensive 'Round-Robin' mechanical test programmes undertaken across several international research institutions [8,9].

The SP test arrangement consists of a miniature disc sample subjected to an applied compressive force transferred through a hemispherical punch indenter onto the upper surface of the disc (Fig. 1). Loading may be applied under a constant force (F), promoting a time-dependent creep type response, or alternatively under a constant rate of displacement, promoting behaviour more akin to tensile deformation. Preliminary investigations into replicating fatigue damage on a SP disc has been conducted by the authors [10], where the force (F) is applied in a cyclic manner until the disc is deemed to have failed. In each of these test arrangements, the compressive loading occurs as the punch tip impacts on the disc sample, promoting a small stage of elastic deformation before leading to the most dominant stage of damage where the membrane around the punch tip begins to stretch. The membrane deforms under biaxial tension leading to a complex and transient stress state, upon which thinning occurs through the cross-section of the material, illustrated for a ductile metallic material in Fig. 2.

This behaviour is in contrast to the stress state witnessed in more conventional test arrangements, where the specimen elongates under an applied uniaxial tensile force until failure. Several publications have discussed proposed methods to correlate the properties generated from SP testing to those from more recognised uniaxial approaches [11–17]. When attempting to correlate ultimate tensile strength (σ_{UTS}) to maximum force (F_{MAX}), several studies have used finite element (FE) simulations to understand the differences in stress state and appropriate methods to compare the properties. Altstadt et al found that the correlation between F_{MAX} and σ_{UTS} cannot be independent of the underlying material properties of the material investigated, which in this case was a range of steels [18]. However, correlations were derived based on the applied small punch force, F_i, which is considered a preferred parameter for estimating σ_{UTS}. Likewise, Holmström et al found that estimations of σ_{UTS} for materials with reduced ductility materials should be undertaken on forces extracted at low deflection (d) values due to the relatively catastrophic nature of plastic deformation experienced in such materials [19]. Garcia et al analysed a wide range of materials and derived several parameters from the SP curve. Attempts were made to correlate the yield strength (σ_y) from a uniaxial tensile curve to an equivalent yield force, or F_e, from the SPT curve. To achieve this correlation, F_e was defined by the crossing point between the SP curve and a straight line parallel to the initial slope of the graph, with an offset d of thickness $(t)/10$ (as shown in Fig. 2(b)). Using this proposal, a regression coefficient α = 0.346 (units in N/mm^2), similar to an R^2 value, was achieved. The most robust correlation was found when estimating σ_{UTS} with F_{MAX}. Here, the authors normalised F_{MAX} by dividing by the initial thickness (t) of the SP disc and the d value at F_{MAX}. However, the proposed correlations between tensile elongation and d at F_{MAX} were generally poor [17]. Hähner et al extended upon this work with effort focused on correlating σ_y from SP testing. They presented a new methodology based on FE simulations of a wide range of constitutive hardening rules based on the reasoning that σ_y is commonly associated with an elastic–plastic transition force (F_e) via $\sigma_y = \alpha \cdot F_e/h^2$. However, they found that the dimensionless coefficient, α, could not be assumed to be constant and depends on the strain hardening behaviour of the investigated material (as similarly reflected by the hardening exponent n of power law flow) which, in the absence of knowledge of n, can be inferred from the curvature of the F-d curve recorded in the SP test. Hähner et al found that this can be achieved by determining the forces at three different offsets (10 μm, 50 μm and 90 μm), rather than attempting to link σ_y to a single offset value [20].

An alternative experimental approach for determining mechanical properties using small specimen discs is the shear punch (ShP) test. In the ShP test, the miniature disc, of equal dimension to that used for SP testing, is clamped between an upper and lower die set in a similar arrangement to SP testing, but force is applied via a flat ended punch rather than a hemi-spherical indenter, promoting a compressive force in the central region of the specimen and a shearing deformation behaviour around the edges of the punch head, and therefore a more uniform stress state throughout the

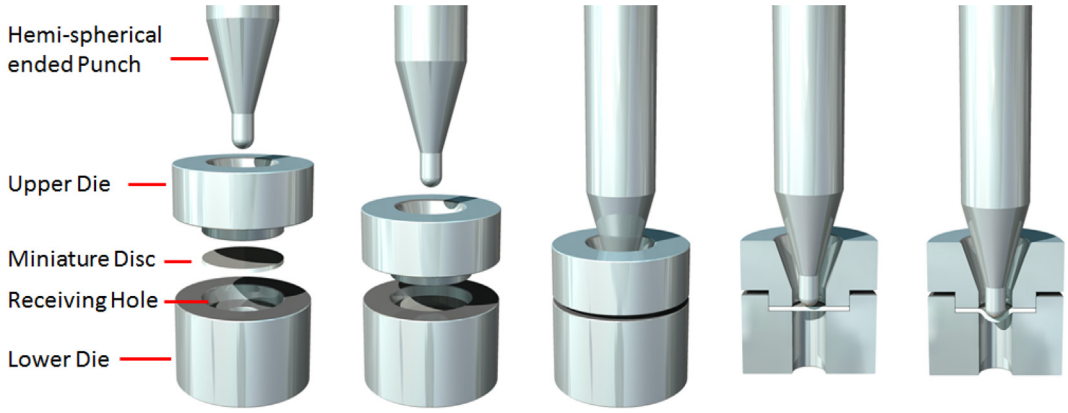

Fig. 1. Small punch test arrangement.

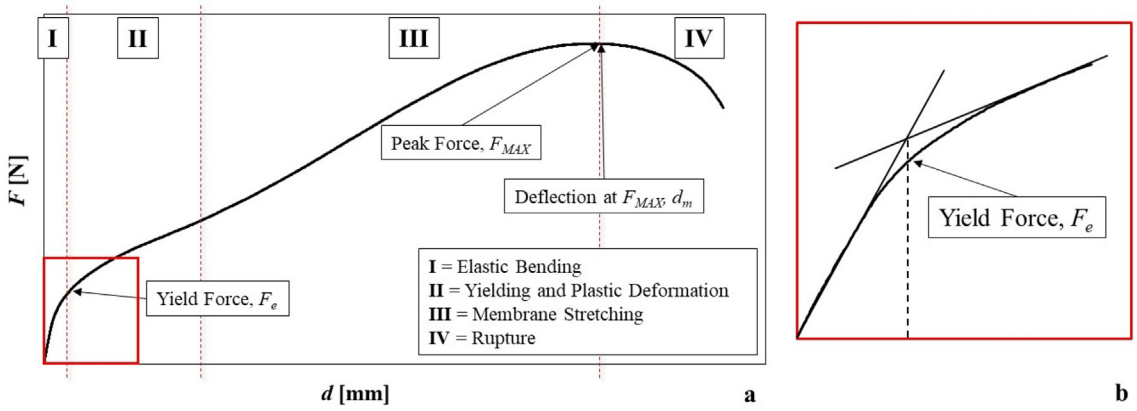

Fig. 2. (a) Example small punch Force-Deflection curve with different deformation zones indicated, (b) Determination of F_e by means of the bilinear method.

test. The specimen is then deformed until a 20% drop from F_{MAX} is reached, producing a *F-d* curve akin to SP testing. The shear stress, τ, is calculated through the following equation:

$$\tau = \frac{F}{2\pi r_{avg} t} \quad (1)$$

where F is the punch load and r_{avg} is the average of the radius of the punch head and the radius of the receiving hole ($r_{avg} = r_{punch} + r_{die} / 2$). The resulting deformation behaviour has many similarities to a σ-ε curve from a uniaxial tensile test, such as an initial linear elastic region, a yield point, a period of plastic deformation until reaching an ultimate load followed by failure, as illustrated in Fig. 3. The exact yield point on the curve is not always easy to define, thus a repeatable method must be employed to calculate the shear yield stress (τ_y). Kobayashi et al found reasonable success when deriving an offset shear yield stress (τ_{PS}) value based on an intersecting point between the τ - d/t curve and a force offset line parallel to the linear portion. In addition, maximum shear stress (τ_{USS}) values could also be established with sufficient correlation to uniaxial properties [21].

Guduru et al adopted the same approach to characterise the mechanical properties of nanocrystalline materials whilst considering a varying specimen thickness and punch to die clearance. The research showed that normalisation of the shear-punch displacement with specimen thickness could produce a SP master curve that is independent of thickness, where using a 0.2% yield offset criterion, a τ_y value can be obtained that correlates strongly with σ_y. Furthermore, good agreement was observed between τ_{USS} and σ_{UTS} [22,23].

The aim of this research was to evaluate the applicability of the SP and ShP test techniques in deriving the mechanical properties of a range of metallic materials with various levels of ductility. Results will be compared and empirically correlated to those generated through more recognised uniaxial means. Finite element analysis simulations will also be presented to analyse the evolving stress fields in the two small scale test approaches, providing further credence to the empirical correlations and helping to identify the limitations of applying small scale test methods to certain metallic materials.

2. Experimental methods

2.1. Materials and specimens

In this study, several wrought crystalline materials were assessed; these were commercially pure copper, commercially pure aluminium, nickel-based superalloy Inconel718 (In718) (53 wt% Ni, 19 wt% Fe, 19 wt% Cr, 4.8 wt% Nb, 3 wt% Mo, 0.86 wt % Ti, 0.60 wt% Al, trace C, S, Cu), titanium alloy Ti-6Al-4V (90 wt % Ti, 6 wt% Al, 4 wt%V, trace Fe, O) and stainless steel 404 (0.05 wt% C, 1.00 wt% Mn, 0.50 wt% Si, 11.5 wt% Cr, 1.5 wt% Ni, 0.03 wt% P, 0.03 wt% S, Bal. Fe). All materials were supplied in the as-received condition, and none were thermo-mechanically treated. The average grain sizes for each material were collected through the mean linear intercept method (displayed in Table 1), each exhibiting an isotropic, equiaxed morphology. 25 individual measurements were taken of each material using ImageJ software.

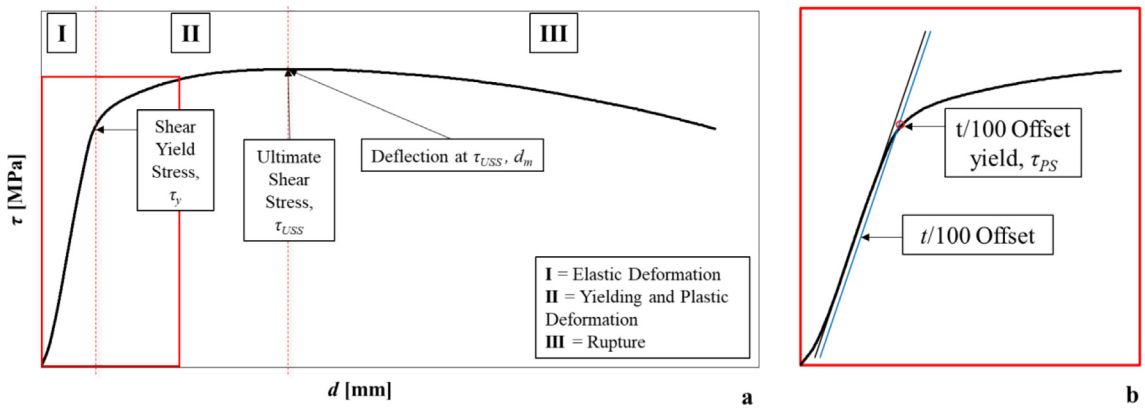

Fig. 3. (a) Example shear punch Force-Deflection curve with different deformation zones indicated, (b) Determination of τ_{PS}.

Table 1
Average grain size measurements for five materials investigated.

Material	Average grain size (μm)
Ti-6Al-4V	3.8
Stainless Steel	6.8
Copper	24.6
Aluminium	38.2
In718	10.0

A series of five uniaxial tensile specimens were manufactured from cylindrical rods from each of the five materials, in accordance with the dimensions given in Fig. 4, with all specimens finished with a circumferential polish. Ten disc specimens (five for SP and five for ShP testing) were then extracted perpendicularly from the same stock of each material by reducing the diameter of the cylinders to ϕ8 mm and sectioning slices approximately 800 μm in thickness. Using a custom designed specimen holder, discs were produced by progressively grinding and polishing both specimen faces with finer silicon carbide abrasive papers to the required specimen thickness of 500 μm ± 5 μm with a 1200 grit finish (Fig. 4(b)). These procedures are in direct accordance with the recommendations defined in the standards for SP testing [8,9].

2.2. Mechanical testing

2.2.1. Uniaxial tensile

Uniaxial tensile tests were performed on a 50 kN electric screw test machine. Across all tests, a constant strain rate of 0.5 mm·min^{-1} was adopted until a strain value of 4 % was exceeded, upon which a second strain rate of 5 mm·min^{-1} was used until failure. All test procedures adhered to ISO6892-1:2016 [24], with 25 data points recorded per second and strain measured through a 12 mm extensometer. All tests were performed in a controlled laboratory temperature of 21 °C.

2.2.2. Small punch tensile

SP tensile tests were performed using a bespoke jig, as previously reported in [6]. The jig assembly locates into a 5kN electric screw test machine and comprises of an upper (2) and lower die (4) set to clamp the SP disc (3), each with a ϕ4 mm receiving hole, as shown in Fig. 5(a)). The lower die holds a 0.2 mm chamfer above the ϕ4 mm receiving hole, with an initial die entrance of ϕ8 mm to avoid obstruction with the punch geometry. When the test frame cross-head is in contact with the flat surface of the push collar, a compressive displacement consequently applies a force to the disc specimen through the punch head. Residual deflection measurements are recorded via an adapted transducer rod which connects the center of the underneath surface of the specimen to a linear variable displacement transducer (LVDT), providing deflection measurements directly from the specimen, to accompany the displacement behaviour recorded from the crosshead movement. All tests were performed in accordance with the EN standard for SP testing [8], under a crosshead displacement rate of 0.5 mm·min^{-1}. Each experiment was performed at ambient room temperature in a controlled laboratory environment (21 °C).

Post test, fractographic images were captured on a Keyence VHX-700F digital microscope, enabled with a stitch image function to allow magnified observations of all regions of the fractured discs.

2.2.3. Shear punch tensile

ShP tests were performed on the same mechanical test frame as the SP tests. All test procedures were akin to those used for SP testing, where the disc (3) is clamped and held in place by an upper (2) and lower die set (4), but the profile and dimensions of the die set and punch indenter differ. Whereas for SP testing the punch (1) contains a hemispherical end, for ShP tests, the punch has a flat profile (as depicted in Fig. 5(b)). As previously shown by Hankin et al [25], the true multiaxial, non-uniform stress state in the annular shear zone, is a relatively uniform shear in conjunction with a small compressive stress. Plus, since there is a widening of the stress field with decreasing stress amplitude outside of the annular region defined by the punch clearance, the combined effect of these multiaxial, non-uniform stresses relative to a pure shear stress state can be accounted for through modifications in the correlation constants connecting the ShP test stresses to uniaxial tensile stresses [25]. As such, Eq. (1) can be adopted as an appropriate definition of τ for the ShP tests. In this research, to be consistent with the work undertaken by Guduru et al [23], a flat end punch of 2.49 mm diameter and a receiving die of 2.51 mm diameter (w = 10 μm) was adopted. Both pieces were manufactured from Nimonic 90. Deflection, displacement and force values were recorded every 0.1 s. To replicate the conditions used for SP testing, all ShP tests were performed with a crosshead displacement rate of 0.5 mm·min^{-1}, in a controlled laboratory temperature of 21 °C.

3. Results & discussion

Figs. 6-8(a) present the typical uniaxial, small punch and shear punch curves for each of the five materials whilst Figs. 6-8(b) show five repeat tests on a given material under each test arrangement. The properties collected from each of the tests is also presented in Table 2, together with the standard deviation values for each property value. For the ShP τ-d curves, τ was derived from F using Eq. (1).

When comparing the individual material responses under each of the different test configurations, it is clear that the underlying behaviours persist despite the contrast in the loading mechanism.

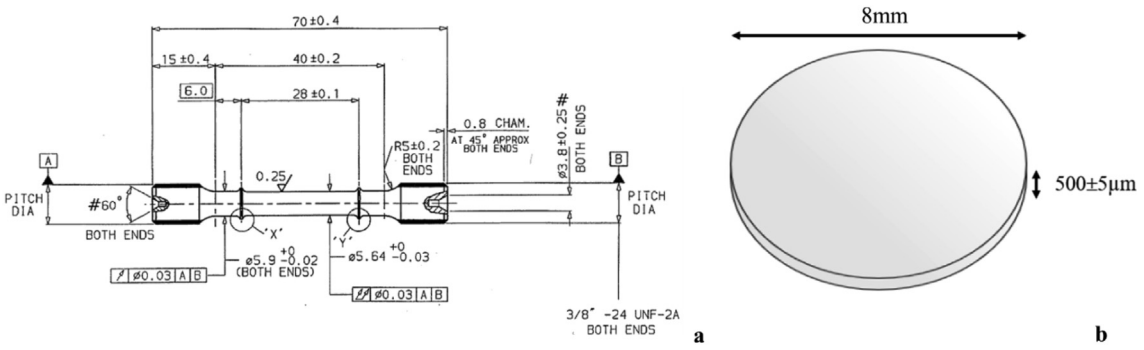

Fig. 4. Test piece geometry for (a) Uniaxial tensile and (b) Small punch and shear punch testing.

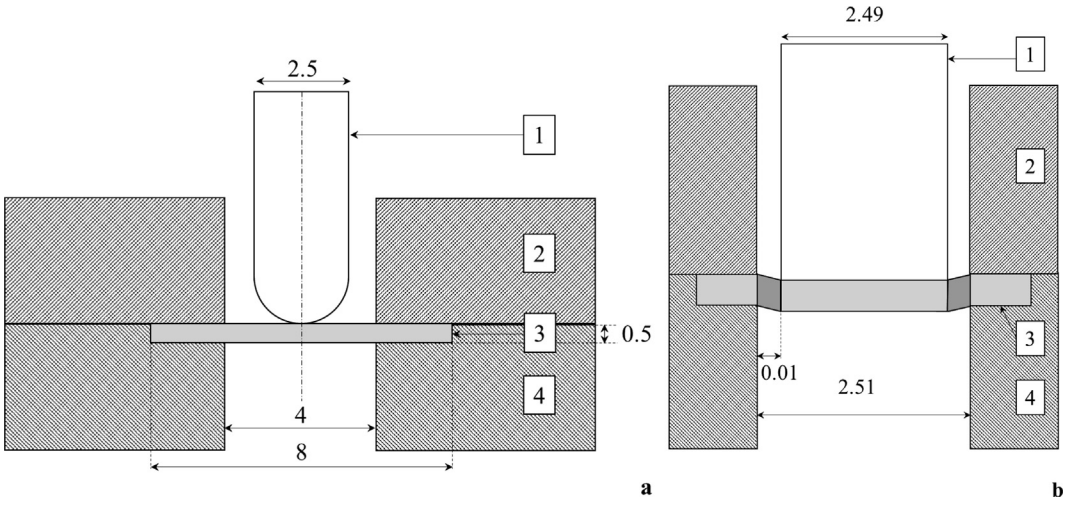

Fig. 5. Schematic of (a) Small punch test, (b) Shear punch test.

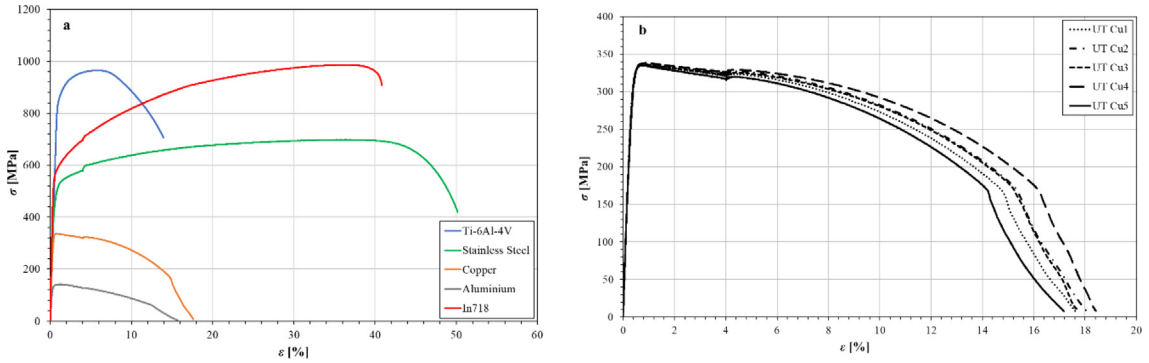

Fig. 6. (a) Uniaxial stress–strain behaviour of five material variants (b) Uniaxial stress–strain behaviour of five repeat tests on copper.

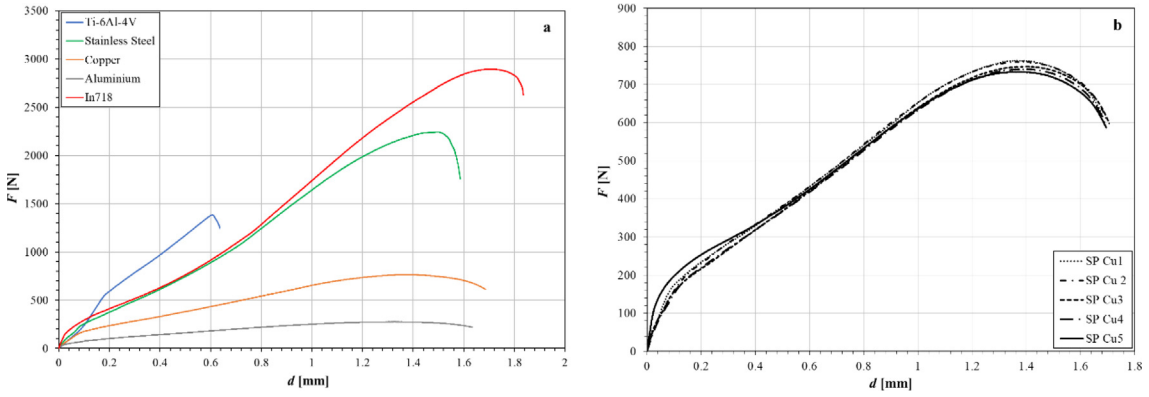

Fig. 7. (a) Small punch force–deflection behaviour of five material variants (b) Small punch force–deflection behaviour of five repeat tests on copper.

For instance, Ti-6Al-4V can be seen have the least ductile response of the five materials across each test type. Under all three tests, Ti-6Al-4V also exhibits the highest point of yielding compared to the other materials, followed by IN718 and stainless steel, which are very similar, then copper and finally aluminium. There is greater scatter in the σ_{UTS} / τ_{USS} values, where for the uniaxial results, the ordering of σ_{UTS} decreases as follows: Ti-6Al-4V, IN718, stainless steel, copper, aluminium. ShP testing reveals a similar ranking, with stainless steel achieving a slightly higher value than IN718. However, under SP conditions, the maximum strength of Ti-6Al-4V is significantly weaker from what would have been expected considering its response under uniaxial and ShP loading.

As the results show, the ShP curves have distinctive stages capturing the different stages of deformation. These include i) an initial period where the shear punch makes contact with the disc at low loads (a stage more prominent in the higher strength materials such as Ti-6Al-4V and IN718), ii) a linear elastic region, iii) a point of deviation in the curve, akin to yield behaviour, iv) a period of non-linear deformation and v) the point of ultimate load, or ultimate shear stress. When comparing these stages to those seen in

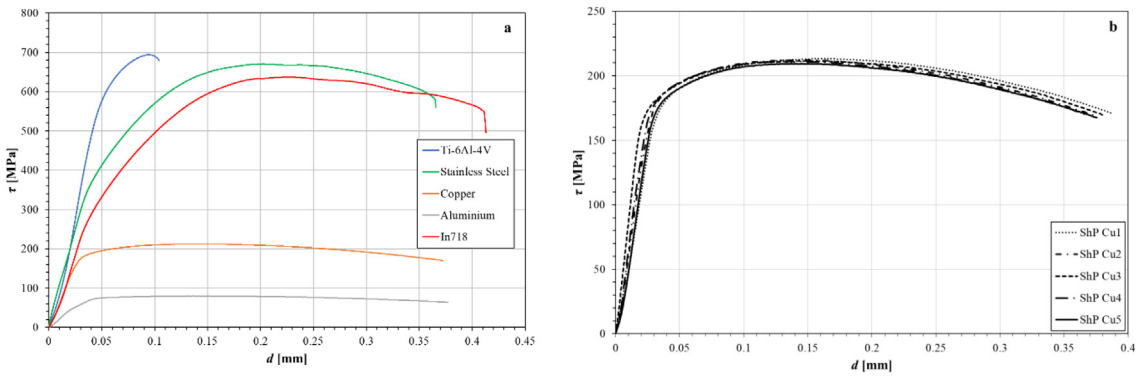

Fig. 8. (a) Shear punch shear stress–deflection behaviour of five material variants (b) Shear punch shear stress–deflection behaviour of five repeat tests on copper.

Table 2
Material properties gathered from uniaxial, small punch and shear punch tensile tests. Standard deviation values across the five tests are given.

	Uniaxial Tensile Results								Small Punch Results						Shear Punch Results					
	σ_{YS}		σ_{PS}		σ_{UTS}		El		F_e		F_m		d_m		τ_y		τ_{USS}		d_m	
	[MPa]		[MPa]		[MPa]		[%]		[N]		[N]		[mm]		[MPa]		[MPa]		[%]	
Ti-6Al-4V	868	36.7	893	28.9	982	14.4	14	1.7	574	76	1384	66	0.6	0.033	572	7.3	674	26.6	0.099	0.009
Stainless Steel	496	12.0	521	18.2	699	1.5	48	0.3	272	37	2280	42	1.5	0.056	415	32.5	661	11.9	0.226	0.016
Copper	316	9.4	334	2.6	337	1.5	18	0.8	147	16	749	13	1.4	0.018	180	3.0	212	1.5	0.147	0.011
Aluminium	127	2.2	137	2.5	142	1.9	16	0.3	58	18	281	14	1.3	0.031	72	1.6	77	3.1	0.135	0.015
In718	545	9.8	561	3.0	986	6.2	37	1.1	237	51	3005	76	1.7	0.014	305	27.8	648	15.9	0.233	0.022

SP testing, stage iii) is typically absent, and as such, definition of a representative yield stress becomes more complex.

3.1. Correlations to uniaxial properties

3.1.1. Small punch

Through the bilinear method as described in the EN standard to obtain the small punch yield force, F_e [8], uniaxial tensile yield stress has previously been estimated from the following relationship:

$$\sigma_y = \alpha_1\left(\frac{F_e}{t^2}\right) + \alpha_2 \tag{2}$$

where α_1 and α_2 are constants derived from linear regression across a series of results and t is the thickness of the specimen at the start of the test. This equation can also be used to define uniaxial proof stress, σ_{PS}, using the same values.

For the estimation of ultimate tensile strength values from the maximum force values generated in a small punch test, F_{MAX}, the following approach has been used:

$$\sigma_{UTS} = \beta_1\left(\frac{F_{MAX}}{t \cdot d_m}\right) + \beta_2 \tag{3}$$

where β_1 and β_2 are constants derived from linear regression and d_m is the deflection at the point of F_{MAX}.

Finally, to estimate percentage elongation, El, values from the deflection at maximum force results, d_m, the following relationship can be adopted:

$$El = \gamma_1 \cdot d_m \tag{4}$$

As shown in Fig. 9, the linear regression relationship between uniaxial properties and results generated through SP testing are highly comparable when considering σ_{PS} and σ_{UTS}, with an R^2 value of 0.93 being achieved in each case respectively. This is despite the considerable change in underlying ductility properties across the five different materials. This difference becomes more of an issue when attempting to correlate uniaxial percentage elongation to the deflection values achieved at the point of maximum force, illustrated in Fig. 9(c). Here, the R^2 value drops to 0.88 and the correlation between the two contrasting data sets is not as clear.

Previous studies have been known to not incorporate α_2 and β_2 setting the y-intercept at the origin, typically related to the resulting goodness of fit (R^2) or average variance in the predicted values compared to the known values. In this research the average variance has been used as the determining factor as to whether constants α_2 and β_2 are used.

3.1.2. Shear punch

Guduru et al found that the definition of shear yield stress could be obtained by using an offset approach on the ShP master curves and comparing these shear yield stress values, τ_y, with uniaxial tensile yield stress values, σ_y [23]. In this research, these terms will be referred to as uniaxial tensile proof stress, σ_{PS}, and shear offset proof stress, τ_{PS}.

When attempting to correlate ShP data with uniaxial properties, a similar approach to equations (2)-(4) can be implemented, as shown in equations (5)-(7), where $m_{1\text{-}3}$ and $n_{1,2}$ are constants that can be determined from a sufficient data series.:

$$\sigma_{PS} = m_1\tau_{PS} + n_1 \tag{5}$$

$$\sigma_{UTS} = m_2\tau_{USS} + n_2 \tag{6}$$

$$El = m_3 d_m \tag{7}$$

Guduru et al found that the shear yield strength corresponding to 1% offset for the materials used in their study produced the best overall correlation with m_1 = 1.77 [23]. Other researchers [26–28] reported an m_1 value of 1.6–2.5 for different material systems. Here, τ_{PS} is correlated directly to σ_{PS}, and the relationship for the five materials was found to be $\sigma_{PS} = 1.4\tau_{PS}$ (R^2 = 0.93), as presented in Fig. 10 (a)). The reason for the discrepancy could be associated with the evolving and additional multi-axial stresses exhibited during shear punch testing. These include the stages of compres-

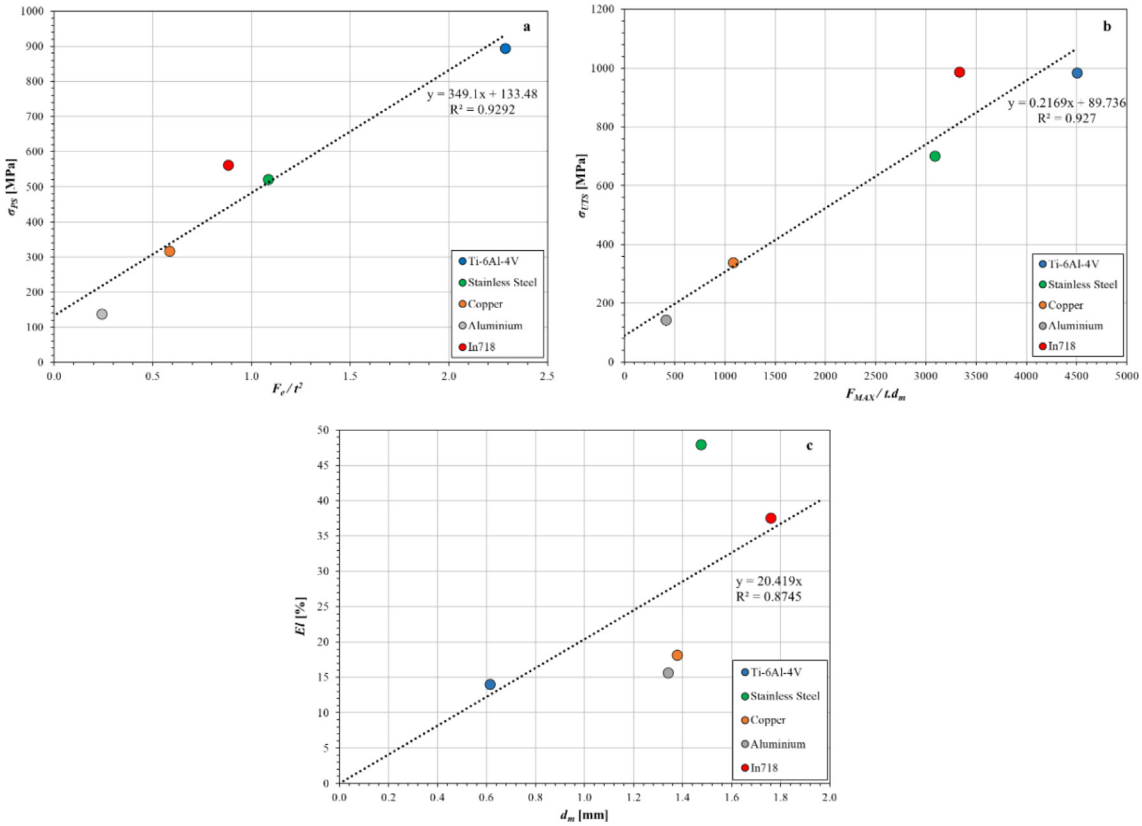

Fig. 9. Comparison of uniaxial and small punch tensile properties for (a) Proof stress, (b) Ultimate tensile stress and (c) Elongation.

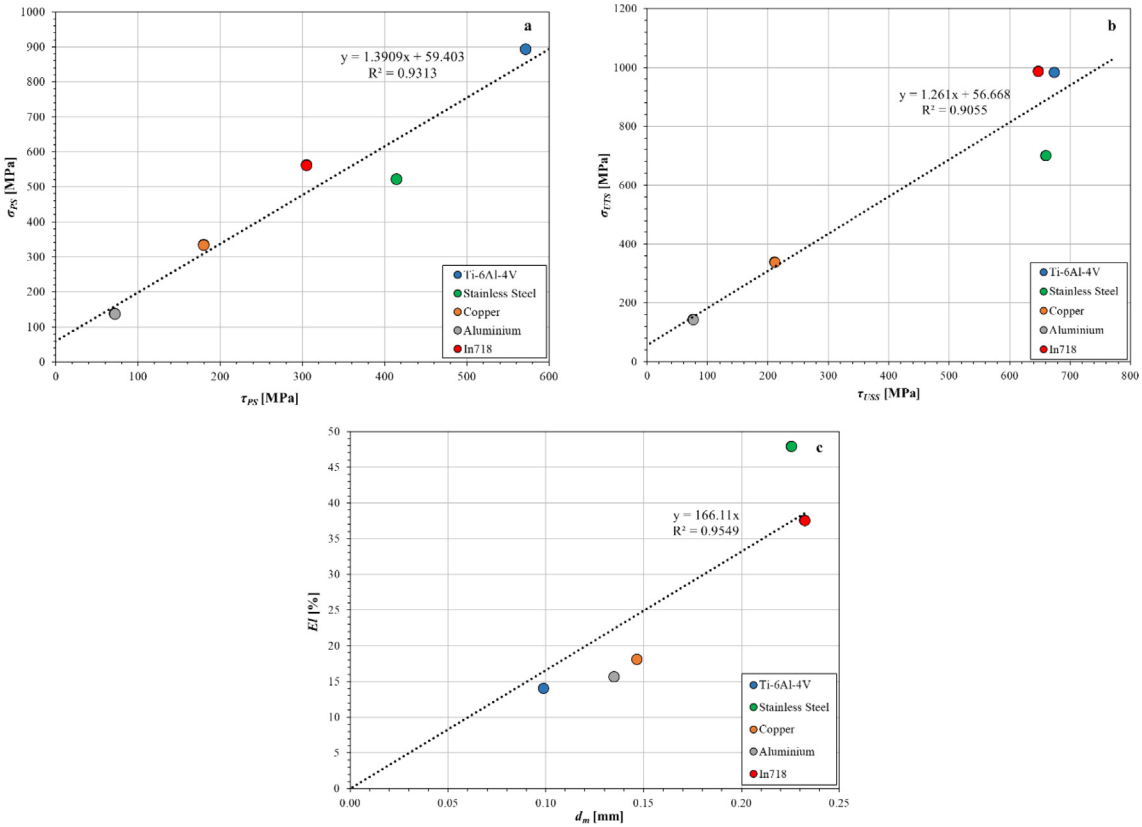

Fig. 10. Comparison of uniaxial and shear punch tensile properties for (a) Proof stress, (b) Ultimate tensile stress and (c) Elongation.

sion, followed by stretching and bending, as the disc material is forced through the receiving hole by the flat headed punch. A similar linear correlation for σ_{UTS} and τ_{USS} was derived by several researchers with m_2 ranging from 1.73 to 2.10 [23,26,28,29]. For the five materials in this research, m_2 = 1.26 (R^2 = 0.91), as shown in Fig. 10(b)). The correlation of total uniaxial percentage elongation to the deflection values achieved at the point of maximum shear stress in an ShP test, is presented in Fig. 10(c)). Here, the R^2 value drops to 0.95. The general fit of the data looks to have improved when compared against the equivalent correlation against SP data, with a clearer trend being established. However, even though the correlation provides a high R^2 value, the linearity of the results is not as strong as that seen for the correlations of σ_{PS} to τ_{PS} and σ_{UTS} to τ_{USS}.

The relationship between the uniaxial results and the predicted results from the SP and ShP tests are presented as unity plots in Fig. 11 with the data given in Table 3. In each case the average variance for the ShP predicted data is less than that for the SP predicted data. For both σ_{PS} and σ_{UTS}, the predictions show a high level of agreement with the properties derived through uniaxial testing, particularly at the lower stress values. The predictions for elongation values however, show far higher scatter in the results and clearly an empirical prediction of this kind can not be deemed suitable in accurately capturing the ductility properties of these materials.

3.2. Finite element analysis

Numerical simulations were performed for the small punch (SP) and shear punch (ShP) configurations on the alloys of interest. For computational efficiency the finite element analysis (FEA) carried-out for each experimental setup was modelled using an axisymmetric analysis, centred about the respective punch axis. The FEA models were constructed in ABAQUS using four-noded bilinear axisymmetric quadrilateral elements, CAX4R. Equivalent approaches have been taken elsewhere in the modelling of both ShP [30] and SP [31], and the hybrid formulation for SP creep testing [32]. In both configurations, the punch and the restraining dies were modelled as discrete rigid bodies and no account is taken for the elastic deformation of the punch and die materials, nor have corrections been made to the simulation results to account for any discrepancies in compliance. The models for both ShP and SP were geometrically the same as those used for testing (Fig. 5) with the exception of increased radii applied to the ShP and the die restraints, from 10 μm to 20 μm; this was chosen for computational convenience.

The elastic constants used in the FEA were derived from a representative data sample generated in the uniaxial tensile tests described previously, and were used in the configurations of both test setups. Whilst it is acknowledged that the Young's modulus (E) values deviate from standard values available, use of the tensile data generated here was deemed necessary for direct comparison of the force response in the ShP and SP scenarios. The input values for E, Poisson's ratio, ν and density, ρ, for the different materials are given in Table 4.

The mesh used in modelling of the ShP setup consisted of 31,000 elements in total. Mesh refinement was applied to the disc workpiece over a width of 500 μm, centred about the clearance zone. The characteristic element size in this refined zone was 5 μm, whereas throughout the rest of the domain a coarser grid

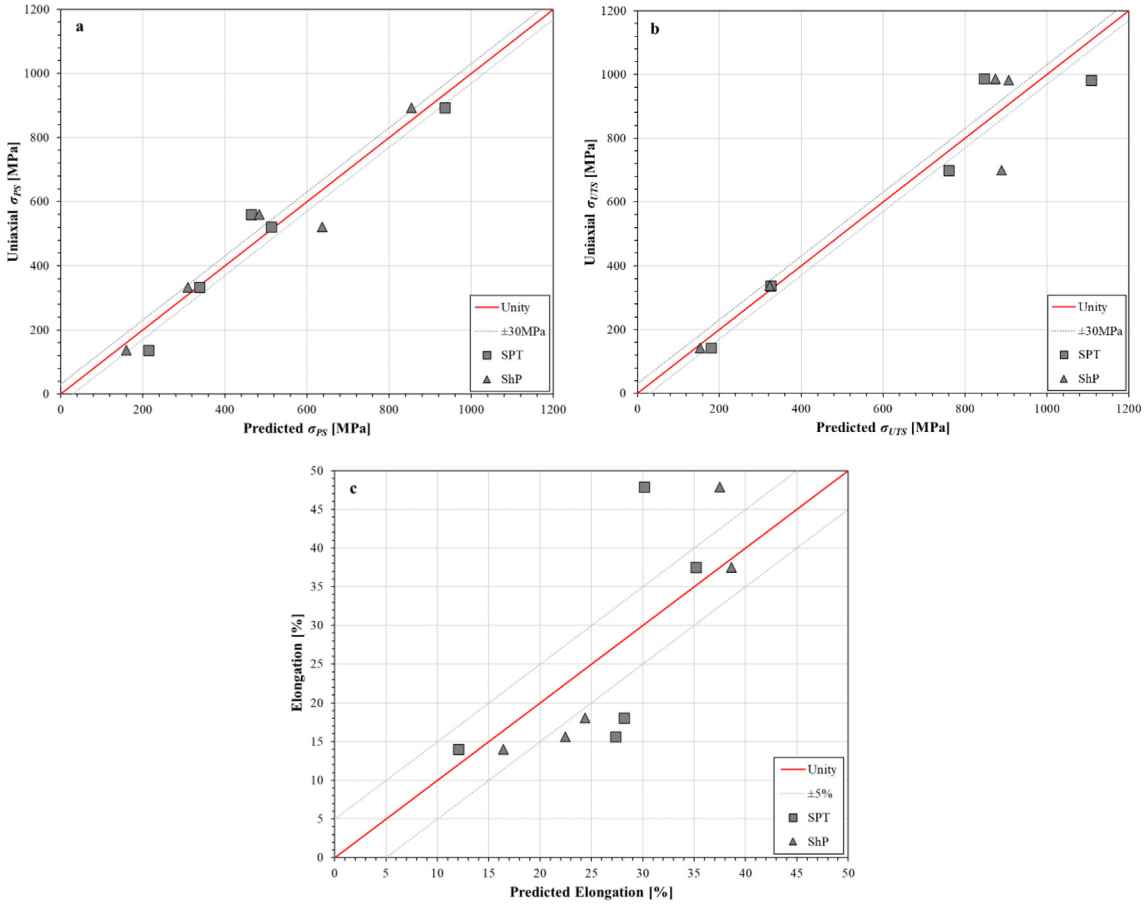

Fig. 11. Unity plots of predicted uniaxial results from SP and ShP correlations for (a) σ_{PS} (b) σ_{UTS} and (c) Elongation.

Table 3
Comparison of uniaxial tensile properties to values predicted from SP and ShP results. Standard deviation and average values across the five tests are given for each data set. The percentage difference between the measured uniaxial and predicted results is also provided.

	Uniaxial Tensile Results				Predicted SP Results						Predicted ShP Results					
	σ_{PS} [MPa]		σ_{UTS} [MPa]		El [%]		σ_{PS} [MPa]	Δ [%]	σ_{UTS} [MPa]	Δ [%]	El [%]	Δ [%]	σ_{PS} [MPa]	Δ [%]	σ_{UTS} [MPa]	Δ [%]	El [%]	Δ [%]
Ti-6Al-4V	893	28.9	982	14.4	14	1.7	936	106.2	–4.8	1108	34.5	–12.8	12.0	0.7	13.9	854	10.2	4.3	907	33.6	7.7	16.4	1.4	–17.4
Stainless Steel	521	18.2	699	1.5	48	0.3	513	51.5	1.5	760	22.0	–8.7	30.1	1.1	37.1	636	45.2	–22.2	890	15.0	–27.2	37.5	2.7	21.7
Copper	334	2.6	337	1.5	18	0.8	338	22.5	–1.4	325	5.9	3.5	28.2	0.4	–55.7	310	4.2	7.1	323	1.9	4.1	24.4	1.8	–34.8
Aluminium	137	2.5	142	1.9	16	0.3	214	24.4	–57.0	181	3.4	–27.0	27.3	0.6	–75.1	160	2.3	–17.0	153	3.9	–7.8	22.4	2.5	–43.7
In718	561	3.0	986	6.2	37	1.1	464	70.8	17.3	847	17.1	14.2	35.2	0.3	6.2	484	38.7	13.7	874	20.0	11.4	38.6	3.7	–3.0

Table 4
Elastic constants and material densities used in simulations.

	E (GPa)	υ	ρ (g/cm^3)
Ti-6Al-4V	122.3	0.34	4.43
Stainless Steel	149.6	0.27	8.00
Copper	94.3	0.35	8.94
Aluminium	55.4	0.34	2.69
In718	170	0.29	8.19

size of 20 μm was used. A similar refinement was made in discretising the rigid bodies, whereby the nodal spacing was reduced around the radii applied. Fixed boundary conditions were applied to the upper and lower die parts and a vertical displacement of the punch was applied at a constant rate throughout the simulation.

In the case of the SP simulation the same principles of mesh refinement were carried through, although here the regions of fine grid sizes were in proximity to the die radii, in addition to another zone of refinement in the free-moving region of the material disc, centred around a point that was remote from the die and the axisymmetric axis, which is an approach similar to that taken in FEA of SP creep elsewhere [33,34]. Again, a characteristic length of 5 μm is enforced in the refined areas, with a coarser grid employed elsewhere in the model. Clearly, given the increased clearance in the SP configuration versus the ShP, bending in the subsequent simulations is expected to be more prevalent than pure shear, although bending is permitted in the ShP setup.

Simulations were performed with a friction coefficient (μ) of 0.75, but since no difference was observed, in all cases, surface-to-surface contact between disc and punch/die was assumed to be frictionless. A series of simplistic material models have been used in ABAQUS CAE, describing the elastic–plastic characteristics of the materials at ambient temperatures, based on uniaxial tensile results given in Fig. 6(a). It is acknowledged that in the absence of a validated damage model, the material models employed are a limitation and the inclusion of sophisticated damage models and genetic algorithms used elsewhere, e.g. [35,36], would be advantageous in evaluating the mechanical behaviour beyond the tensile strengths of the materials. As such, consideration of the simulation results is limited to Mises stresses prior to the maximum exhibited strength of the material. The material flow curves used in the simulations are shown in Fig. 12.

The shear stress values calculated using Eq.1 are given for the ShP simulations and presented in Fig. 13. An offset has been applied for clarity of viewing, whereby the start of each curve is separated by a 0.02 mm interval to allow the individual curves to be fully appreciated. It is noted that the quoted displacements are much smaller than those experimentally derived, which has been observed elsewhere and attributed to the higher stiffnesses associated with the use of rigid bodies [30]. The order of τ_{PS} values can be seen to follow that of the experimental results and the derived values are in reasonable agreement with the mechanical tests performed, which are representative of the material inputs for the models. As is seen in the tensile data, the greatest degree of hardening prior to the τ_{USS} value is exhibited by IN718, whereas the more ductile, less alloyed materials – commercially pure aluminium and copper – show limited hardening and only moderate ductility under ShP testing prior to reaching the τ_{USS} value.

The evolution of the shear stress fields and the associated plasticity measure, PEEQ, are shown in Fig. 14 for one of the materials of interest – stainless steel – at a deflection corresponding to the peak shear stress present, equivalent to those predicted at yield, and 75% of the maximum predicted shear stress. The shape and form of the predicted plastic zones are in good agreement with other published results [30] and show a moderate width of the ele-

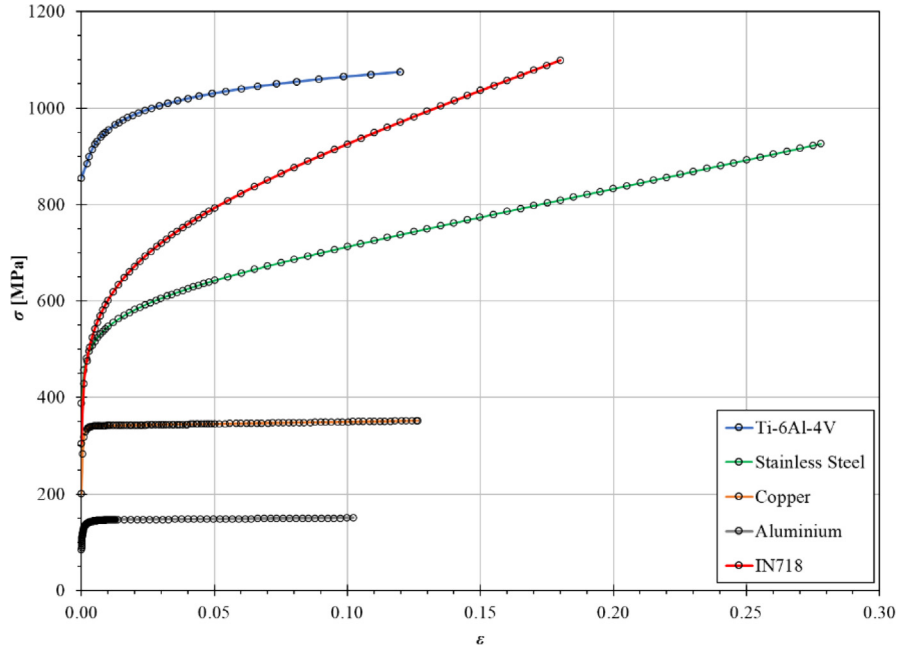

Fig. 12. Model material stress–strain curves used in FEA.

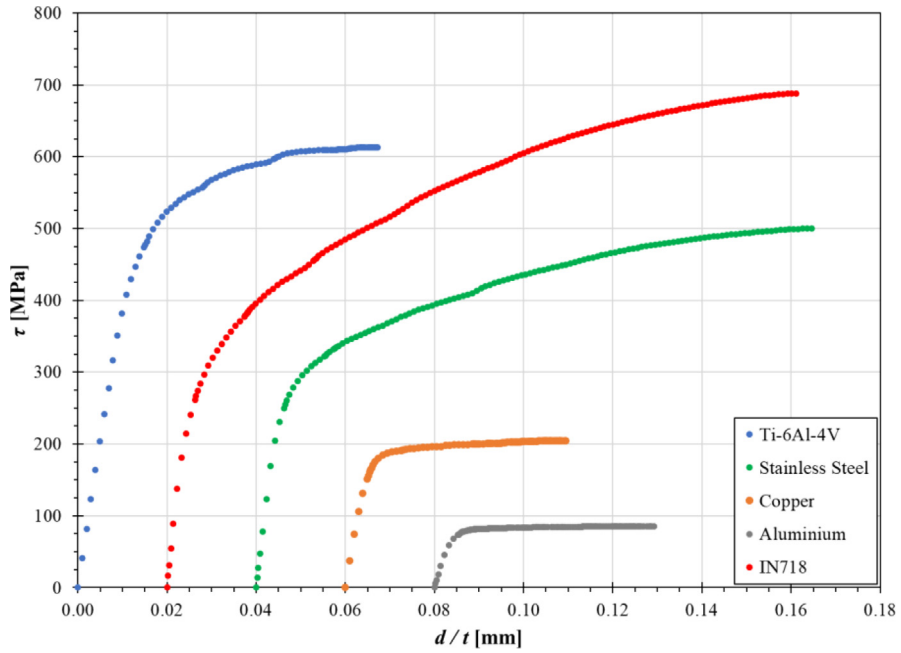

Fig. 13. ShP curves obtained from FEA simulations.

vated shear stress band both at τ_{PS} and close to τ_{USS}. The equivalent plastic strain can be seen to be confined close to the contact between the shear punch specimen and the rigid bodies close to yield and extend through the specimen thickness at larger deformations centred around the clearance zone. In all cases, the shear stress levels throughout the simulated tests are limited to a material-specific shear band width with the majority of the specimens experiencing relatively low stress levels, confining the interpretation of the data from this type of test to this highly directional deformation on a relatively small volume of material.

A comparison between the IN718 alloy and the commercially pure copper specimens under ShP conditions is presented in Fig. 15, where the predicted Von Mises stresses are given at τ_{PS}, independent of the applied deflection. The difference between a ductile material and a highly alloyed material is demonstrated clearly here, where the width of the peak stress band is increased for the more hardenable IN718 alloy (Fig. 15(a)) than that for the near-pure elemental copper specimen. In both cases, the peak Von Mises stresses stretch from the flat extremity of the punch to an equivalent position on the die. However, additional peak stresses are observed on the upper and lower faces of the specimen under the punch in the case of IN718, although in the experimental tests no significant evidence of deformation was observed, nor failure from these positions.

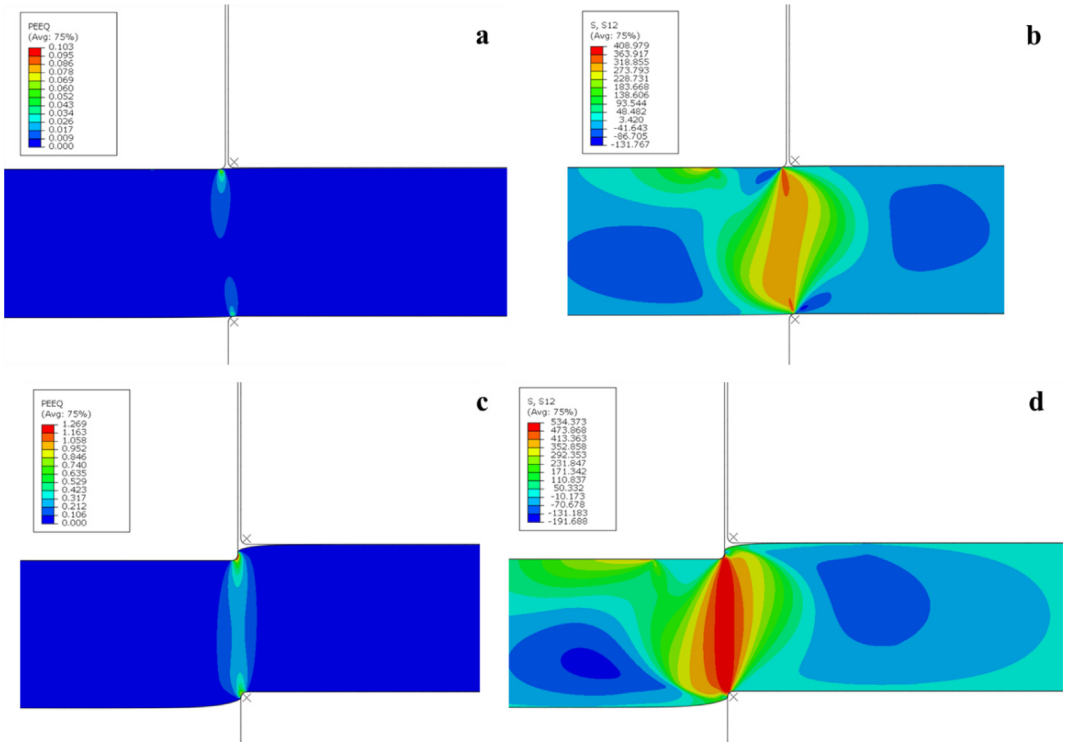

Fig. 14. PEEQ and σ_{rz} contours for stainless steel simulation at (a-b) τ_{PS}, and (c-d) 75% τ_{UTS}.

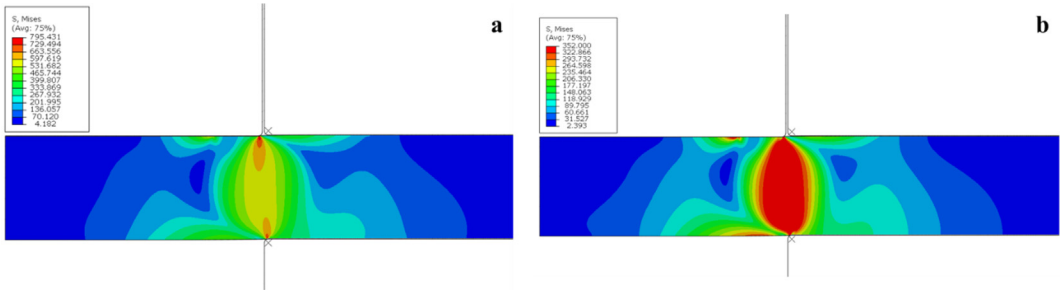

Fig. 15. Mises stress contours at yield for simulations on (a) IN718, and (b) Copper.

The correlation between the predicted τ_{PS} and the experimentally determined σ_{PS} in tensile tests is given in Fig. 16 (a). A strong trend can be seen to exist between the measured tensile and simulated shear data with a factor close to $\sqrt{3}$, which is in agreement to the experimentally derived relationship determined in this investigation and given in [23] where materials of similar behaviour were investigated. In terms of comparison between predicted shear stress results (calculated from simulated reaction loads using Eq. (1)) and the τ_{USS} observed in ShP tests (average given in Fig. 16 (b)), there is reasonable correlation between simulation and experimental values, with a slightly reduced predicted τ_{USS} than observed. This discrepancy may be a result of unoptimized mesh parameters or the limitations of the material model inputted from the tensile data up to the limit of the tensile stress only. Again, no damage parameters have been introduced into the FE model and as such there is likely to be a higher degree of error present at large deflections and stresses. The greatest discrepancy in the data seen in Fig. 6(b) is the data point corresponding to stainless steel, although it is acknowledged that the variance in determination of τ_{PS} in the presence of experimental take-up and in the absence of a correction applied elsewhere [23] is likely to influence the values determined.

The results from simulations performed using the SP configuration and the same material models is given in Fig. 17, describing the reaction forces predicted as a function of the applied punch deflection. The *F-d* curves follow those derived in experimentation (to the limit of the material model, σ_{UTS} shown in Fig. 17) and the order of the F_{MAX} values predicted is in line with what would be expected, although a greater deviation in the simulated behaviour between the IN718 alloy and the stainless steel materials is predicted versus that observed in SP testing, particularly at smaller punch displacements. The resultant curve for the Ti-6Al-4V material is given in Fig. 17(b) for the experimentally determined *F-d* results and the numerical simulation. It can be seen in experimentation, the range of deflection is considerably lower than the other materials, and indeed less than would be expected considering the

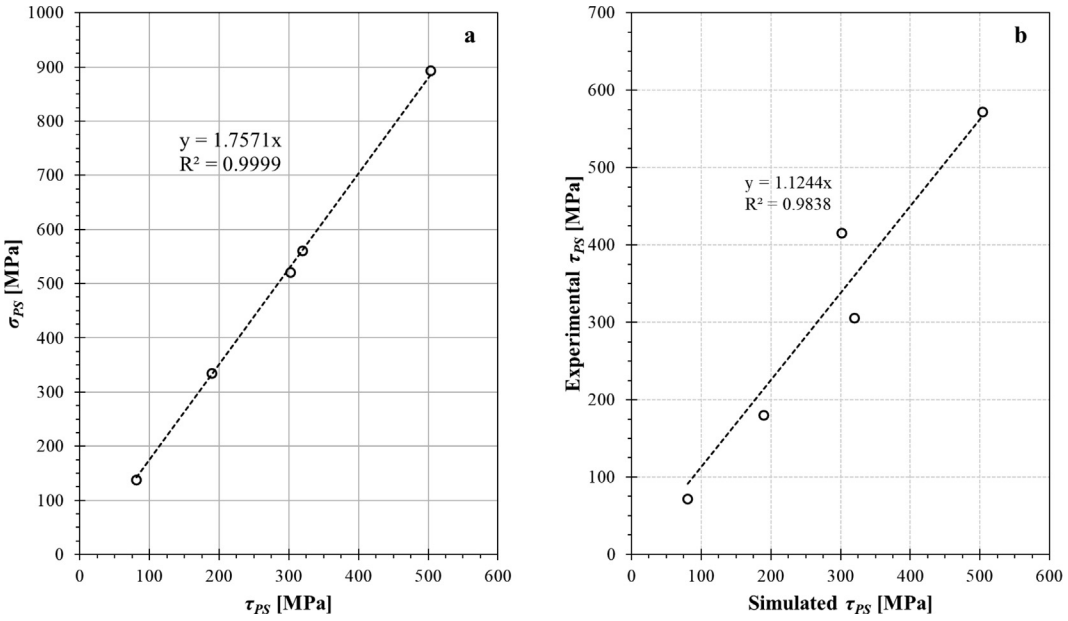

Fig. 16. (a) Correlation between FEA ShP τ_{PS} data and average uniaxial σ_{PS} tensile test data, and (b) Experimentally determined τ_{PS} versus FEA prediction.

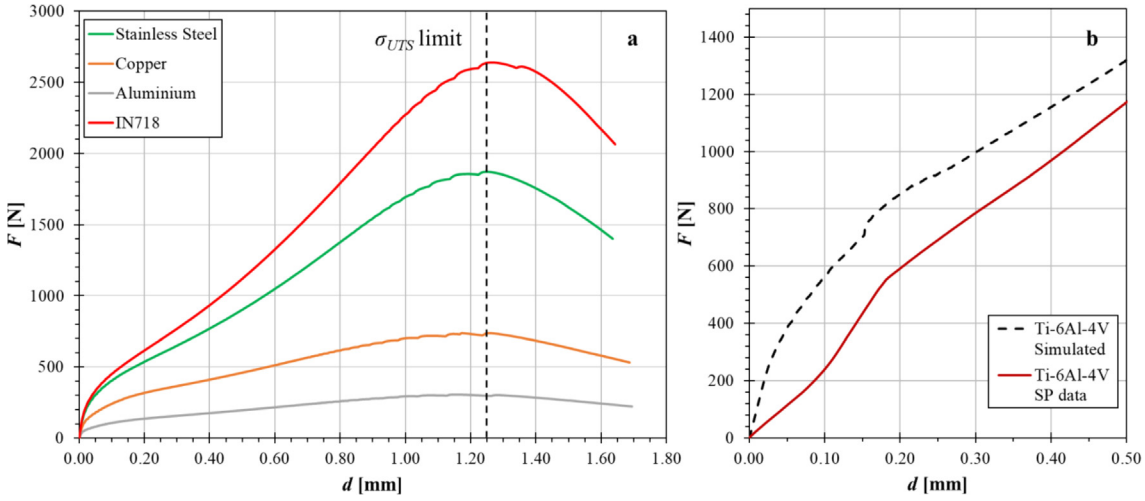

Fig. 17. Reaction force versus displacement (a) results of simulated SP setup for four of the alloys of interest, and (b) Ti-6Al-4V simulated vs. experimental SP force–deflection.

generated tensile data in isolation. In contrast, the simulated *F-d* curve for Ti-6Al-4V shows a form that is consistent with the results predicted for the other materials of interest.

Shear stress fields and Von Mises stress contours predicted by FEA are given in Fig. 18 for IN718 and Ti-6Al-4V at a deflection of 0.5 mm. It can be seen that the areas of peak shear stress induced at this deflection is far more prevalent in the Ti-6Al-4V material (Fig. 18(a)) than in the IN718 material (Fig. 18(c)), spanning from the tangent of the punch to the radius of the rigid die. In terms of Von Mises stress at this deflection, the bulk of the material under bending is experiencing a maximum value, in contrast to IN718 (Fig. 18(b)) where the maximum Von Mises stress is limited to the disc material directly below the advancing punch. This rapid rise in stress for material in unsupported areas of the test piece, with a relatively small applied deflection, may be the cause of the Ti-6Al-4V material being unsuitable for testing in the small punch test configuration under these test conditions, i.e. 0.5 mm/min. It is also important to consider the hexagonal close packed (HCP) crystal structure of Ti-6Al-4V and the reduced number of readily available slip systems in the material. Given that the stress-state in SP testing is far more complex and continuously evolving as compared to uniaxial and ShP deformation, Ti-6Al-4V could potentially be unsuitable for SP testing due to the material's low ductility and the reduced number of available mechanisms of slip. Also given in Fig. 18 is the equivalent plastic strain field, PEEQ, for each simulation at this deflection, and it is seen that the plastic strain accumulated in Ti-6Al-4V (Fig. 18(d)) is coincident to the location observed in IN718 (Fig. 18(b)). However, it is more confined in area and its angle is more acutely orientated relative to the deformed specimen.

Fig. 19 shows typical macro-scale images of the fractures of the SP specimens for each of the tested materials. In general, a large degree of plasticity is observed for four of the materials (aluminium, copper, IN718 and stainless steel) in the form of dimpling, and a defined thinned circumferential region is present, accompanied by the fracture. In the case of the Ti-6Al-4V, a much smoother bottom surface of the test piece is observed, with cracking to a larger scale. The deformation behaviour of Ti-6Al-4V is known to be

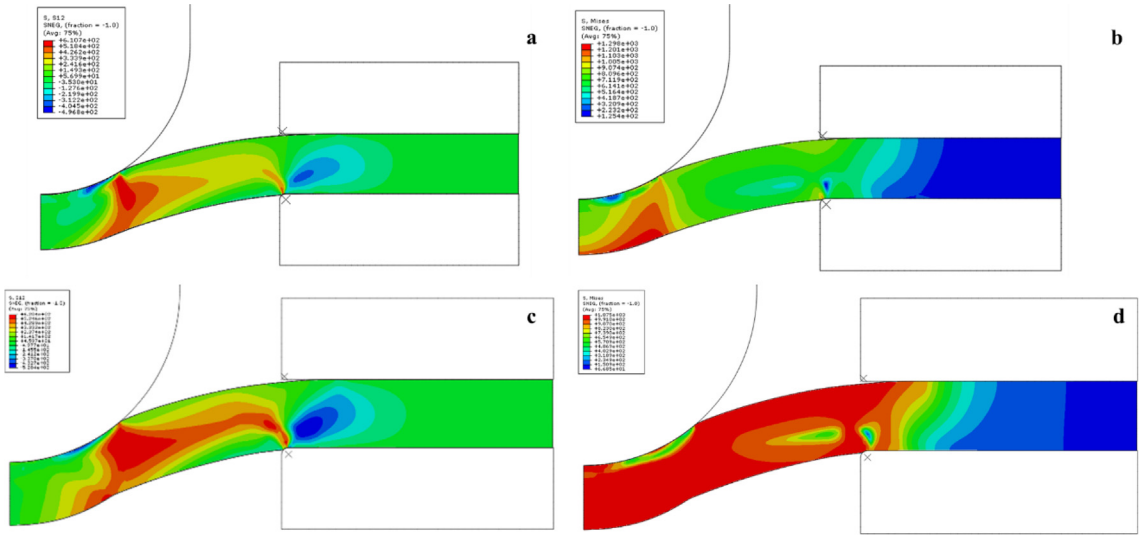

Fig. 18. Predicted σ_{rz} and Mises stresses in SP simulations on (a-b) IN718, and (c-d) Ti-6Al-4V taken at a displacement of 0.5 mm; PEEQ fields at equivalent displacements are shown inset.

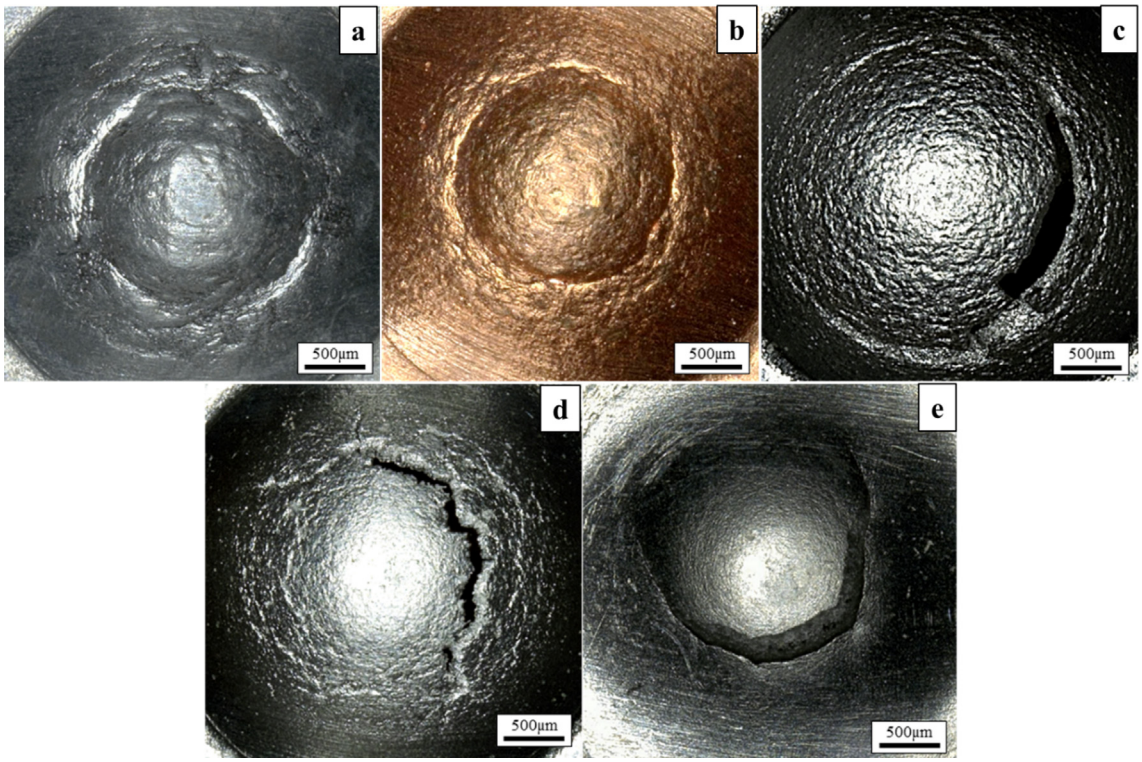

Fig. 19. Fractured small punch (SP) specimens for (a) aluminium, (b) copper, (c) IN718, (d) stainless steel and (e) Ti-6Al-4V, captured using a Keyence VHX-700F digital microscope.

sensitive to both strain rate and temperature under high strain [37] and quasi-static [38] conditions and the failure mechanism is known to change – grain boundary sliding, shear band formation – depending upon the grain size and testing conditions, such as temperature, strain rate and applied strain.

4. Conclusions

The research presented in this paper has examined the suitability of determining tensile properties of a selection of metallic materials using small punch (SP) and shear punch (ShP) test approaches. The materials used for this study included copper, aluminium, stainless steel, IN718 and Ti-6Al-4V. From this research, the following conclusions can be drawn:

- Linear relationships between data sets generated from SP, ShP and uniaxial tensile test methods have been proven, producing regression coefficients of comparable similarity to those published in the current literature. Correlations between ultimate tensile stress and proof stress properties and their respective SP and ShP equivalents were particularly strong, obtaining R^2 values > 0.91.

- Unity plots displaying the relationship between the experimental uniaxial results and the empirically derived predicted properties from the SP and ShP tests showed a high level of agreement for ultimate tensile stress and proof stress properties. In each case, the properties predicted from the ShP results offered a stronger fit.
- Finite element modelling has been shown to capture the deformation behaviour of both SP and ShP test types, up to the point of maximum force. The simulations of the SP test revealed that for a relatively small applied deflection, a significant rise in stress in unsupported areas of the test piece was seen in Ti-6Al-4V. This behaviour was observed in isolation to the other materials, and can be attributed to the HCP crystal structure of the material and the reduced number of readily available slip systems, thus leading to a reduction in ductility. This behaviour was corroborated by post test fracture analysis, where ductile dimpling and gross plasticity was observed in copper, aluminium, stainless steel and IN718, yet these features were absent in Ti-6Al-4V.

Data Availability

The raw/processed data required to reproduce these findings cannot be shared at this time as the data also forms part of an ongoing study.

Declaration of Competing Interest

The authors declare that they have no known competing financial interests or personal relationships that could have appeared to influence the work reported in this paper.

References

[1] M.P. Manahan, A.S. Argon, O.K. Harling, The development of a miniaturized disk bend test for determination of post irradiation mechanical properties, J. Nucl. Mater. 104 (1981) 1545–1550.

[2] R.C. Hurst, R.J. Lancaster, S.P. Jeffs, M.R. Bache, The contribution of small punch testing towards the development of materials for aero-engine applications, Theor. Appl. Fract. Mech. 86 (2016) 69–77, https://doi.org/10.1016/j.tafmec.2016.07.013.

[3] M. Fernández, C. Rodríguez, F.J. Belzunce, T.E. García, Use of small punch test to estimate the mechanical properties of powder metallurgy products employed in the automotive industry, Powder Metall. 58 (3) (Jul. 2015) 171–177, https://doi.org/10.1179/0032589915Z.000000000242.

[4] S.P. Jeffs, R.J. Lancaster, T.E. Garcia, Creep lifing methodologies applied to a single crystal superalloy by use of small scale test techniques, Mater. Sci. Eng. A 636 (2015) 529–535, https://doi.org/10.1016/j.msea.2015.03.119.

[5] R.J. Lancaster, S.J. Davies, S.P. Jeffs, D.T.S. Lewis, M.P. Coleman, The effects of thermal exposure on the high temperature behaviour of a laser powder bed fused nickel based superalloy C263, Mater. Sci. Eng. A. 801 (2021) 140409, https://doi.org/10.1016/j.msea.2020.140409.

[6] S. Davies, S. Jeffs, R. Lancaster, G. Baxter, High temperature deformation mechanisms in a DLD nickel superalloy, Materials 10 (5) (2017) 457, https://doi.org/10.3390/ma10050457.

[7] CEN Workshop Agreement CWA 15267, "European Code of Practice: Small Punch Test Method for Metallic Materials." CEN Members National Standards Body, pp. 1–69, 2007.

[8] "BS EN 10371:2021 Metallic materials - Small punch test method," pp. 1–60, 2021.

[9] "ASTM 61832 Standard Test Method for Small Punch Testing of Metallic Materials," pp. 1–12, 2020, doi: 10.1520/E3205-20.2.

[10] R.J. Lancaster, S.P. Jeffs, H.W. Illsley, C. Argyrakis, R.C. Hurst, G.J. Baxter, Development of a novel methodology to study fatigue properties using the small punch test, Mater. Sci. Eng. A 748 (2019) 21–29, https://doi.org/10.1016/j.msea.2019.01.074.

[11] E. Altstadt, H.E. Ge, V. Kuksenko, M. Serrano, M. Houska, M. Lasan, M. Bruchhausen, J.-M. Lapetite, Y. Dai, Critical evaluation of the small punch test as a screening procedure for mechanical properties, J. Nucl. Mater. 472 (2016) 186–195, https://doi.org/10.1016/j.jnucmat.2015.07.029.

[12] C. Soyarslan, B. Gülçimen, S. Bargmann, P. Hähner, Modeling of fracture in small punch tests for small- and large-scale yielding conditions at various temperatures, Int. J. Mech. Sci. 106 (2016) 266–285, https://doi.org/10.1016/j.ijmecsci.2015.12.007.

[13] M.F. Moreno, Effects of thickness specimen on the evaluation of relationship between tensile properties and small punch testing parameters in metallic materials, Mater. Des. 157 (2018) 512–522, https://doi.org/10.1016/j.matdes.2018.07.065.

[14] I.I. Cuesta, J.M. Alegre, M. Lorenzo, Influence of strain state in mechanical behaviour of aluminium alloys using the Small Punch Test, Mater. Des. 54 (Feb. 2014) 291–294, https://doi.org/10.1016/j.matdes.2013.08.038.

[15] M. Bruchhausen, S. Holmström, I. Simonovski, T. Austin, J.-M. Lapetite, S. Ripplinger, F. de Haan, Recent developments in small punch testing: Tensile properties and DBTT, Theor. Appl. Fract. Mech. 86 (2016) 2–10, https://doi.org/10.1016/j.tafmec.2016.09.012.

[16] M. Fernández, C. Rodríguez, F.J. Belzunce, T.E. García, Use of small punch test to estimate the mechanical properties of sintered products and application to synchronizer hubs, Met. Powder Rep. 72 (5) (2017) 355–360, https://doi.org/10.1016/j.mprp.2016.02.056.

[17] T.E. García, C. Rodríguez, F.J. Belzunce, C. Suárez, Estimation of the mechanical properties of metallic materials by means of the small punch test, J. Alloys Compd. 582 (Jan. 2014) 708–717, https://doi.org/10.1016/j.jallcom.2013.08.009.

[18] E. Altstadt, M. Houska, I. Simonovski, M. Bruchhausen, S. Holmström, R. Lacalle, On the estimation of ultimate tensile stress from small punch testing, Int. J. Mech. Sci. 136 (2018) 85–93, https://doi.org/10.1016/j.ijmecsci.2017.12.016.

[19] S. Holmström, I. Simonovski, D. Baraldi, M. Bruchhausen, E. Altstadt, R. Delville, Developments in the estimation of tensile strength by small punch testing, Theor. Appl. Fract. Mech. 101 (2019) 25–34, https://doi.org/10.1016/j.tafmec.2019.01.020.

[20] P. Hähner, C. Soyarslan, B. Gülçimen Çakan, S. Bargmann, Determining tensile yield stresses from Small Punch tests: A numerical-based scheme, Mater. Des. 182 (2019) 107974, https://doi.org/10.1016/j.matdes.2019.107974.

[21] T. Kobayashi, Y. Miura, M. Yamamoto, "Tensile property evaluation of a Japanese reactor pressure vessel steel by Shear punch test technique, in: Proceedings of 5th International Small Sample Test Techniques Conference, 2018.

[22] R.K. Guduru, K.A. Darling, R.O. Scattergood, C.C. Koch, K.L. Murty, M. Bakkal, A.J. Shih, Shear punch tests for a bulk metallic glass, Intermetallics 14 (12) (2006) 1411–1416, https://doi.org/10.1016/j.intermet.2006.01.052.

[23] R.K. Guduru, K.A. Darling, R. Kishore, R.O. Scattergood, C.C. Koch, K.L. Murty, Evaluation of mechanical properties using shear-punch testing, Mater. Sci. Eng. A 395 (1–2) (2005) 307–314, https://doi.org/10.1016/j.msea.2004.12.048.

[24] "ISO 6892-1:2016 Metallic materials — Tensile testing — Part 1: Method of test at room temperature," pp. 1–79, 2016.

[25] G.L. Hankin et al., An Investigation into the Origin and Nature of the Slope and x-axis Intercept of the Shear Punch-Tensile Yield Strength Correlation using Finite Element Analysis, in: M.L. Hamilton, A.S. Kumar, S.T. Rosinski, M.L. Grossbeck (Eds.), Effects of Radiation on Materials: 19th International Symposium, ASTM International, West Conshohocken, PA, 2000, pp. 1018–1028.

[26] M.L. Hamilton, M.B. Toloczko, G.E. Lucas, Recent progress in shear–punch testing, in: Proceedings of International symposium on miniaturized specimens for testing of irradiated materials, 1994, pp. 46–51.

[27] G.L. Hankin, M.B. Toloczko, M.L. Hamilton, R.G. Faulkner, Validation of the shear punch–tensile correlation technique using irradiated materials, J. Nucl. Mater. 258–263 (1998) 1651–1656, https://doi.org/10.1016/S0022-3115(98)00203-7.

[28] M.B. Toloczko, R.J. Kurtz, A. Hasegawa, K. Abe, Shear punch tests performed using a new low compliance test fixture, J. Nucl. Mater. 307–311 (2002) 1619–1623, https://doi.org/10.1016/S0022-3115(02)01258-8.

[29] M.L. Hamilton, M.B. Toloczko, Effect of low temperature irradiation on the mechanical properties of ternary V-Cr–Ti alloys as determined by tensile tests and shear punch tests, J. Nucl. Mater. 283–287 (2000) 488–491, https://doi.org/10.1016/S0022-3115(00)00227-0.

[30] R.K. Guduru, R.O. Scattergood, C.C. Koch, K.L. Murty, A.V. Nagasekhar, Finite element analysis of a shear punch test, Metall. Mater. Trans A 37 (5) (2006) 1477–1483.

[31] R.J. Lancaster, H.W. Illsley, G.R. Davies, S.P. Jeffs, G.J. Baxter, Modelling the small punch tensile behaviour of an aerospace alloy, Mater. Sci. Technol. 33 (9) (2016) 1065–1073, https://doi.org/10.1080/02670836.2016.1230168.

[32] F. Cortellino, J.P. Rouse, B. Cacciapuoti, W. Sun, T.H. Hyde, Experimental and numerical analysis of initial plasticity in P91 steel small punch creep samples, Exp. Mechanics. 57 (8) (2017) 1193–1212.

[33] J.P. Rouse, F. Cortellino, W. Sun, T.H. Hyde, J. Shingledecker, Small punch creep testing: review on modelling and data interpretation, Mater. Sci. Technol. 29 (11) (2013) 1328–1345, https://doi.org/10.1179/1743284713Y.0000000278.

[34] Y.W. Ma, S. Shim, K.B. Yoon, Assessment of power law creep constants of Gr91 steel using small punch creep tests, Fatig. Fract. Eng. Mater. Struct. 32 (12) (2009) 951–960.

[35] E. Martínez-Pañeda, I.I. Cuesta, I. Peñuelas, A. Díaz, J.M. Alegre, Damage modeling in small punch test specimens, Theor. Appl. Fract. Mech. 86 (2016) 51–60, https://doi.org/10.1016/j.tafmec.2016.09.002.

[36] V.D. Vijayanand, M. Mokhtarishirazabad, Y. Wang, M. Gorley, D.M. Knowles, M. Mostafavi, Estimating damage parameters of a CuCrZr alloy subjected to two

varying heat treatments using small punch test, J. Nucl. Mater 557 (2021) 153263, https://doi.org/10.1016/j.jnucmat.2021.153263.
[37] W.S. Lee, C.F. Lin, Plastic deformation and fracture behaviour of Ti–6Al–4V alloy loaded with high strain rate under various temperatures, Mater. Sci. Eng. A 241 (1–2) (1998) 48–59, https://doi.org/10.1016/S0921-5093(97)00471-1.
[38] W. Zhou, K. Chew, The rate dependent response of a titanium alloy subjected to quasi-static loading in ambient environment, J. Mater. Sci. 37 (23) (2002) 5159–5165, https://doi.org/10.1023/A:1021085026220.